Clay Minerals (2024), **59**, 11–21
doi:10.1180/clm.2024.2

Article

Green and solvent-free fabrication of conductive halloysite–polythiophene nanocomposites for the removal of organic pollutants from aqueous media

Golshan Samee[1], Nasser Arsalani[1], Saeideh Same[2], Golnaz Navidi[3] and Hasan Kalantar Esfangare[1]

[1]Department of Organic Chemistry and Biochemistry, Faculty of Chemistry, University of Tabriz, Tabriz, Iran; [2]Research Center for Pharmaceutical Nanotechnology, Tabriz University of Medical Sciences, Tabriz, Iran and [3]Department of Chemistry and Biochemistry, University of Oregon, Eugene, OR, USA

Abstract

Toxic pharmaceutical pollutants, such as nicotine, represent a significant threat to natural water sources due to their continuous discharge. To address this issue, clay minerals and their composites have demonstrated exceptional adsorptive and remedial capabilities for wastewater purification. This research focused on developing green clay-polymeric adsorbents for the efficient removal of pharmaceutical pollutants from industrial wastewater. The synthesis involves creating halloysite nanotube–polythiophene nanocomposites through a green and cost-effective method using vapour polymerization and a solvent-free, ball-milled technique for the adsorptive removal of nicotine from wastewater. The investigation evaluates the impacts of preparation, modification and environmental conditions on the adsorptive performance of these clay-based nanocomposites compared to pure polythiophene. The polymerization process was evaluated by varying the vapour polymerization holding time for a fixed amount of oxidant ($FeCl_3$) and halloysite nanotube (HNT) to investigate the impacts of monomer vapour exposure time on the polymerization of nanocomposites. Following the characterization of the synthesized adsorbents using various methods, the study investigated the impacts of various parameters (e.g. adsorbent dosage, pH and contact time) on the adsorption capabilities of the materials on a laboratory scale. The results revealed that the incorporation of HNT improved the adsorbing performance of nanocomposites. The pH, absorbent concentration and contact time directly affect nicotine adsorption. Significantly, halloysite–polythiophene 3 with a 2 h polymerization duration demonstrated the maximum adsorption efficacy of 78.94% at pH 10 after a 24 h contact time. The environmentally friendly halloysite-based nanocomposite shows promising potential as an effective adsorbent for pharmaceutical pollutant (nicotine) removal from aquatic environments.

Keywords: Adsorbent, environmental chemistry, green chemistry, halloysite nanotube, nicotine removal

(Received 18 September 2023; revised 28 December 2023; Accepted Manuscript online: 24 January 2024; Associate Editor: Chunhui Zhou)

The continuous release of hazardous and carcinogenic chemical substances into water sources could lead to irreversible damage to the environment and all living organisms if this is not urgently addressed (Dutta & Rana, 2019; Kumar *et al.*, 2023). Nicotine, a poisonous water pollutant, is commonly delivered into wastewater from industries such as those involved in tobacco and smoking products, pharmaceuticals (as a licit drug for replacement therapies), insecticide factories, agriculture and domestic extractions by smokers (Anastopoulos *et al.*, 2020; Verovšek *et al.*, 2022). Nicotine, a toxic tobacco alkaloid, is a psychoactive drug that affects the nervous system and mental functioning (Mohan *et al.*, 2021). Consequently, its residual presence in wastewater, and ultimately in natural rivers, lakes and seawater, contaminates clean water supplies and raises global ecotoxicological concerns due to its psychoactive characteristics (Oropesa *et al.*, 2017; Jin *et al.*, 2022). Given its solubility and stability in water, it is crucial to develop a novel, cost-effective, efficient adsorbent with a simple manufacturing process and high capacity to remove nicotine from wastewater effluents, ensuring safe water access for all living organisms (Koutela *et al.*, 2020).

Among a wide variety of adsorbents, the clay minerals, known for their mechanical and chemical stability, have gained attention for their application in nanocomposite preparation for the effective sorption of contaminants (Masindi *et al.*, 2021). In particular, halloysite nanotubes (HNTs), a type of aluminosilicate ($Al_2Si_2O_5(OH)_4.2H_2O$) tubular nanoclay, have been recognized as a green nanomaterial for chemical and biological studies and applications (Ma *et al.*, 2018). Abundantly present in the natural environment, HNTs present a remarkable surface area-to-volume ratio, cation-exchange capacity (CEC), biocompatibility, water-holding capacity and fast adsorption rate (Same *et al.*, 2022b). HNTs, with their unique characteristics of opposite surface charges (having a negatively charged outer surface and a positively charged inner surface of the tube lumen), have the ability to selectively adsorb cationic or anionic materials onto their surface or lumen (Nyankson & Kumar, 2019). As a result, HNTs have been widely utilized as economical and unconventional adsorbents in various research projects for the removal of water contaminants under various environmental circumstances (Zhao & Liu, 2008; Capsoni *et al.*, 2022). Pure HNTs demonstrated fast and effective adsorption

Corresponding author: Nasser Arsalani; Email: arsalani@tabrizu.ac.ir
Cite this article: Samee G, Arsalani N, Same S, Navidi G, Kalantar Esfangare H (2024). Green and solvent-free fabrication of conductive halloysite–polythiophene nanocomposites for the removal of organic pollutants from aqueous media. *Clay Minerals* **59**, 11–21. https://doi.org/10.1180/clm.2024.2

of various dyes such as Methyl Violet and Neutral Red from an aqueous solution (Zhao & Liu, 2008; Luo *et al.*, 2010). Furthermore, the sorption capacity of raw minerals such as HNTs can be improved by incorporating them into appropriate polymeric networks (Nguyen *et al.*, 2019; Niu *et al.*, 2023).

Polymeric composites have been extensively used in water purification due to their ease of development, functionalization, low cost, simple application and high removal efficacy (Dutta & Rana, 2019). Aromatic conjugated polythiophene (PTh) and its nanocomposites are a particularly favoured group of polymeric adsorbents due to their environmental compatibility, thermal stability, non-toxicity, high conductivity, large surface area, porous structure and reversible ion-sorption capability (Haghgir *et al.*, 2022). PThs are synthesized through a simple and cost-effective procedure, readily allowing for them to be scaled up (Dutta & Rana, 2019).

Using a nanocomposite material consisting of HNTs and conductive polymers is expected to enhance the removal of pharmaceuticals through adsorption processes. The aim of this study was to assess the potential of combining the characteristic features of HNTs and polymers in a single platform to improve their great applicability for contamination removal and rapid wastewater treatment. To achieve this, a new multifunctional nanocomposite was successfully developed by utilizing for the first time HNTs as a supportive nanostructure for thiophene polymerization following an ecofriendly and solvent-free procedure. This approach was conducted to combine the mechanical and sorption capabilities of HNT clays with the thermal stability, conductivity and adsorption efficacy of PTh. The use of supportive HNTs for the immobilization of a biomimetic catalyst *via* the polymerization of aniline has also been reported previously (Tierrablanca *et al.*, 2010). The high-energy ball-milling technique was applied to fabricate the HNT-PTh nanocomposite *via* the vapour polymerization process, which is a direct, solvent-free and green method. This green fabrication procedure offers significant advantages of cost-effectiveness, operational simplicity, mild reaction conditions, short reaction times, high yields and easy workup processes. The present research specifically focused on the removal of nicotine, as a representative organic pollutant, from aqueous solution. The structures of the fabricated nanocomposites were thoroughly characterized using various analytical techniques, including Fourier-transform infrared (FTIR) spectroscopy, scanning electron microscopy (SEM), energy dispersive X-ray spectroscopy (EDX), thermogravimetric analysis (TGA) and X-ray diffraction (XRD) analyses. Additionally, the effects of initial polymerization holding time, adsorbent dosage, contact time and pH on adsorption efficiency were investigated.

Experimental

Materials

The thiophene monomer (C_4H_4S, $\rho = 1.06$ kg L^{-1}), ferric chloride ($FeCl_3$, molecular weight (MW) = 162.21 g mol^{-1}) and HCl were obtained from Merck Chemical Co. (Darmstadt, Germany). Nicotine (MW = 162.23 g mol^{-1}) was purchased from ChemNovatic Co. (Lublin, Poland). Halloysite (with a diameter of 30–70 nm, length of 1–3 µm and CEC of 8) was supplied by Sigma-Aldrich (Saint Louis, MO, USA).

Pre-treatment of halloysite nanotubes

Approximately 500 mg of raw halloysite clay was milled (clay/ball ratio: 1/6) using a ball-milling machine (Ball-Milling Model MM400, Retsch, Germany) equipped with 50 mL of stainless steel double-walled ball mill beaker and two stainless steel balls of 7 mm in diameter and with a weight of 1500 mg. Dry ball milling was performed at a frequency of 15 Hz at room temperature for 30 min.

Green solvent-free synthesis of the HNT-PTh nanocomposite

The electrically conductive HNT-PTh nanocomposites were prepared in two steps based on the green conditions of vapour-phase monomer polymerization (Enzel & Bein, 1989; Acharya *et al.*, 2010). First, 150 mg of $FeCl_3$ (oxidant and dopant) and 350 mg of HNT were poured into a stainless steel double-walled ball mill beaker equipped with two stainless steel balls (7 mm in diameter/1500 mg weight) and ball milled at 15 Hz frequency for 30 min (Teimuri-Mofrad *et al.*, 2016). In the second step, the obtained milled yellow powder was exposed to thiophene monomer vapour directly for predetermined durations in a closed air-tight flask at room temperature (composite/ball ratio: 6/1; Fig. 1). The progress of polymerization was identified by the colour change of the powders from yellowish to brown–black.

Thereafter, the resultant blackish HNT-PTh powders were rinsed thoroughly with distilled water and ethanol to remove any residual ferric chloride. Finally, the obtained brown–black precipitates were separated by centrifugation and dried at room temperature. The colour change and dark appearance of nanocomposite powders after washing indicated successful polymerization and doping. The nanocomposites were prepared after 30 min, 1 h and 2 h of exposure to monomer vapour, which are specified as HNT-PTh1, HNT-PTh2 and HNT-PTh3, respectively. The preparation of pure PTh, without HNT, was performed

Figure 1. Air-tight polymerization flask aiming to expose the yellow-milled HNT-$FeCl_3$ powder to monomer vapours.

https://doi.org/10.1180/clm.2024.2 Published online by Cambridge University Press

by following the same procedure for comparison. All samples have been prepared in triplicate.

FTIR spectroscopy

The chemical characterizations and functional groups of the HNT, PTh and polymerized nanocomposites were determined using an FTIR spectrophotometer (Bruker Model TENSOR 27, Germany). The infrared absorption spectra of all prepared KBr sample pellets – a pressed mixture of 99 mg KBr and 1 mg sample – were scanned over the wavenumber range of 400–4000 cm^{-1} (Bordeepong *et al.*, 2011).

XRD analysis

The crystalline structures of the samples were investigated using XRD (Bruker AXS D8 Discover Diffractometer, Germany) techniques and International Centre for Diffraction Data (ICDD) crystallographic databases. The XRD traces of prepared specimens were measured using a Siemens D-500 diffractometer at the scan rate of 1 min^{-1} over a scan range of 5–70°2θ with Cu-*K*α radiation (λ_{max} = 1.5406 Å) operating at 30 kV and 20 mA. Bragg's law was used to calculate the basal spacings of the halloysite nanotubes before and after mixing them with PTh in composites.

$$2d\sin\theta = n\lambda \quad (1)$$

In Equation 1, d is the diffracting plane (basal) spacing, θ is the diffraction angle and $n = 1$ (relevant crystal plane; Ismail *et al.*, 2008; Aresta *et al.*, 2011).

SEM and EDX analyses

The morphologies of the HNTs, PTh and HNT-PTh nanocomposites were visualized using SEM (MIRA3 FEG-SEM, Tescan, Czechia). Samples were covered with a thin Au–Pd layer by a sputter coater (Polaron SC7620, Quorum Technologies, UK) before examination by SEM. The presence and distribution of elements on the surfaces of the polymer and nanocomposites were assessed by employing EDX (MIRA3 FEG-SEM, Tescan, Czechia). The analysed samples were cut and mounted on electron microprobe stubs (Hokmabad *et al.*, 2018; Same *et al.*, 2022b).

Thermogravimetric analysis

The thermal stabilities of the HNTs, PTh and HNT-PTh nanocomposites were evaluated using TGA (Linseis L81A1750, Germany) under an N_2 atmosphere from room temperature to 800°C at a heating rate of 10°C min^{-1}. Weight loss percentage was calculated from the residual mass at 800°C (Cheng *et al.*, 2010).

Electrical resistivity

Electrical conductivity was measured using the standard four-probe method (under dry conditions) *via* a specific resistivity adapter (Keithley, Model 4210, 1100 V source meter, USA) at room temperature using compressed pellets of dry sample powders. Each reported value was calculated from the average of three resistivity measurements (Yu *et al.*, 2005).

Point of zero charge measurement

The point of zero charge (pHpzc) determination was conducted on the HNT-PTh composite through the salt addition method (Holliman *et al.*, 2008). Initially, solutions of 0.1 M NaCl were prepared and their pH adjusted to the range of 2–10 with 0.1 M NaOH and HCl solutions. Then, 0.1 g of obtained composite was added to 20 mL of the solution and mixed thoroughly at room temperature for 24 h. The pH values of the samples were recorded (Digital Sartorius pp-15 pH meter, Germany) and the difference between the initial and final pH (ΔpH) was plotted against the initial pH.

Adsorption investigations

The effects of the influential independent experimental variables and operating parameters including the adsorbent dosage (50 or 100 mg), contact time (5 or 24 h) and various pH values (2, 7, 9, 10, 11 or 13) on nicotine removal were studied. A total of 24 tests were performed on each prepared nanocomposite (HNT-PTh1, HNT-PTh2 and HNT-PTh3) and also compared with the adsorption performance of PTh and pristine HNT. Analyses were carried out in 50 mL beakers, each of which containing 10 mL of prepared nicotine-contaminated water (nicotine solutions: 20 mg L^{-1} of nicotine in distilled water) at various pH values. Then, specific amounts of the adsorbents were added to the beaker, and the mixture was stirred homogeneously at room temperature for a predesignated period of contact time. Finally, the solutions were centrifuged and the concentrations of nicotine adsorption were determined using an ultraviolet spectrophotometer (Unico 2100, S2100 SUV, NJ, USA) at the maximum wavelength of nicotine (261 nm) within the wavelength range 300–700 nm. The pH of the test solutions was adjusted with HCl (0.1 M) or NaOH (0.1 M).

Statistical analysis

The tests were analysed using *t*-tests and analysis of variance (ANOVA) assays in triplicate. All results were represented as the mean ± standard deviation (SD), and $p < 0.05$ was considered statistically significant.

Results and discussion

The rapid growth of both the global population and industrialization has resulted in increasing environmental pollution and water resource contamination, posing serious threats to human health. This study sought to address these concerns by synthesizing HNT-enriched PTh nanocomposites using a green and eco-friendly polymerization method in the presence of $FeCl_3$. Subsequently, the synthesized HNT-PTh nanocomposites were utilized for the adsorption of nicotine from aquatic environments (Fig. 2).

Synthesis

The fabrication of novel nanocomposite adsorbents involved a mechanical ball-milling reaction performed under green, clean and solvent-free conditions. This process enabled the vapour polymerization of PTh on the surface of HNTs with the goal of chemically purifying polluted water. This green chemistry technique allowed for direct and environmentally friendly

https://doi.org/10.1180/clm.2024.2 Published online by Cambridge University Press

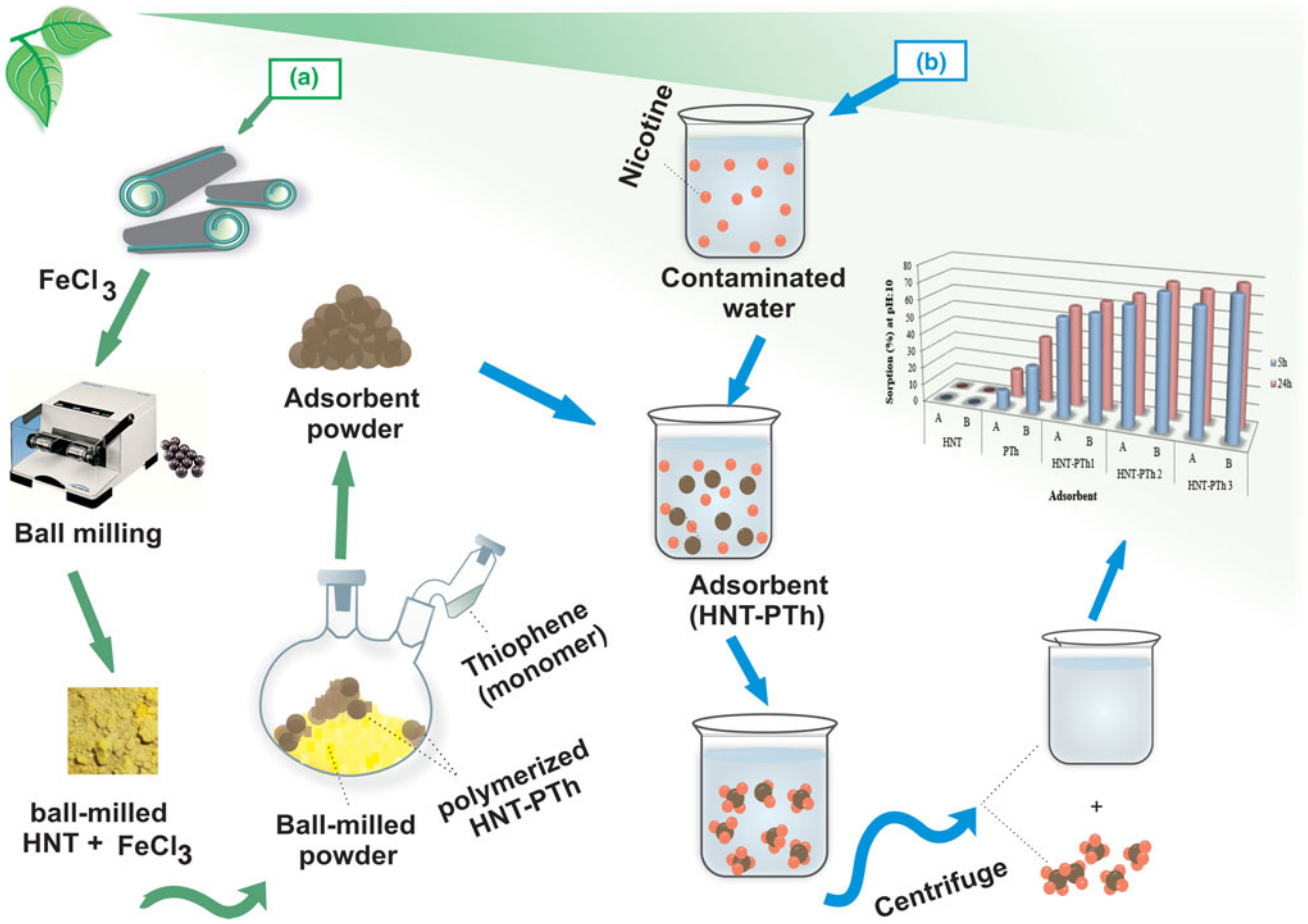

Figure 2. Schematic illustration of the HNT-enriched PTh nanocomposite preparation following a green polymerization process and evaluation of its adsorption potential in aqueous media. (a) Following the ball milling of HNT powder in the presence of $FeCl_3$, HNT-PTh composites were polymerized by exposing the obtained ball-milled HNT-$FeCl_3$ powder to thiophene (monomer) vapour. (b) Prepared nanocomposites were mixed with contaminated water and employed for the removal of nicotine under various experimental circumstances. Ultimately, the applied nanocomposites were separated using a centrifuge, and the efficacy of the adsorbents for the removal of nicotine was investigated using the cleaned water.

polymerization on HNT surfaces without needing to use harsh acidic/basic media, high polymerization temperatures, high energy consumption, hazardous energy sources (high radiation) or toxic solvents (Arsalani *et al.*, 2009). Conventional synthesis methods, by contrast, often require the use of organic solvents, leading to significant challenges due to the formation of poisonous substances that have destructive effects on the ecosystem and public health (Ghadiri *et al.*, 2020).

The results confirmed that the amount of monomer vapour (increasing exposure time from 30 min to 2 h) directly influenced the amount of vapour polymerization, as HNT-PTh3 exhibited the highest degree vapour polymerization (45.2 mg) compared to HNT-PTh1 (43.8 mg). Additionally, the findings indicated that the employed polymerization process rapidly progressed without the need for high temperatures (heating) or prolonged reaction times, as evidenced by the immediate colour change of the examined powder mixture from yellow to black upon exposure to thiophene monomer vapours. This green polymerization method allowed for the synthesis of HNT-PTh nanocomposites under simple conditions, eliminating hazardous solvents and the expensive, time-consuming manufacturing processes associated with conventional methods, thereby indicating promise for industrial application.

FTIR spectroscopy analysis

The chemical structures of the HNT powder, synthesized PTh and prepared HNT-PTh were studied using FTIR spectroscopy. In the HNT spectrum (Fig. 3), the absorption peak at 3620 cm^{-1} was attributed to O–H stretching of inner hydroxyl groups, whereas that at 3697 cm^{-1} was related to O–H stretching of interlayer Al–OH groups. The absorption peaks at 749 and 790 cm^{-1} were indexed to Si–O network stretching. Additionally, the band at 911 cm^{-1} corresponded to the O–H bending of Al–OH, and the peaks at 1037 and 537 cm^{-1} were associated with in-plane Si–O stretching, whereas the absorption band of the O–H deformation of water was observed at 1650 cm^{-1} (Zahedi *et al.*, 2012). In the synthesized PTh spectra, the absorption peak of C = S stretching was found at 1334 cm^{-1} (Sulub *et al.*, 2009). Moreover, the peak at 790 cm^{-1}, characteristic of α,ά-coupling of poly-2,5-thiophene and the vibration of the thiophene ring, signified the effective polymerization of the thiophene monomer (Khanmohammadi & Babazadeh, 2018).

Finally, the absorption bands of the C = C stretching vibration and C–S bending vibration were specified at 1450–1600 and 749 cm^{-1}, respectively (Lu & Yang, 2005; Gnanakan *et al.*, 2009). In the infrared spectra of the HNT-PTh nanocomposites,

https://doi.org/10.1180/clm.2024.2 Published online by Cambridge University Press

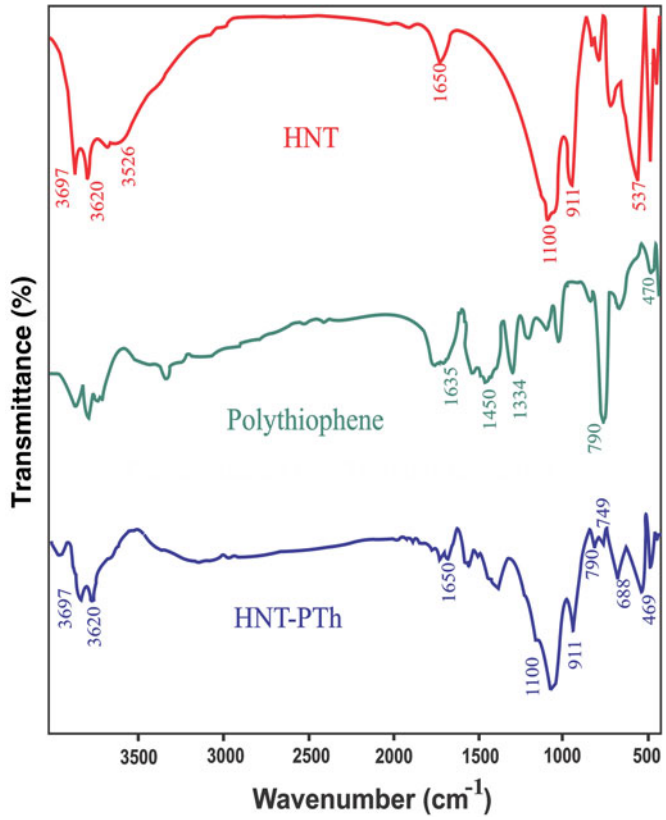

Figure 3. FTIR spectra of HNT-PTh, PTh and HNTs.

the most distinctive absorption bands of each component of the composites appeared in the expected areas, providing evidence that the HNT and PTh nanocomposites had successfully formed.

TGA analysis

The thermal stability of prepared compounds was determined *via* thermal weight analysis. In Fig. 4, the TGA diagrams of the prepared PTh and HNT-PTh are presented. The curve representing PTh, synthesized *via* vapour polymerization in the presence of an oxidant, indicates a one-step decomposition process. PTh exhibited degradation at ~300°C due to the degradation of polymer chains, with an increased weight loss at higher temperatures (>550°C; Sulub *et al.*, 2009; Khanmohammadi & Babazadeh, 2018). The thermal resistance of the polymerized composites increased after incorporating HNTs. It is proposed that the existence of tubular halloysites with large lumens delays the thermal decomposition of polymeric nanocomposites and decreases mass transportation due to the entrapment of residual degradation products.

As the findings show, the HNT-PTh composite samples exhibited weight loss at four stages, each being due to a distinct thermal-based process. The initial mass loss could be related to the evaporation of the interlayer water of HNTs (Sahnoune *et al.*, 2017). The second stage of decomposition at ~400°C is associated with polymer degradation, inducing a higher temperature of decomposition than that of pure PTh (Acharya *et al.*, 2010). The subsequent weight loss at ~500°C was related to the dihydroxylation and condensation reactions of the hydroxyl groups of HNTs (Sahnoune *et al.*, 2017; Cheng *et al.*, 2020). Finally, the maximum level of decomposition of polymeric nanocomposites is shifted towards a higher value (600°C) compared to that of pure PTh. As such, it can be concluded that embedding halloysite into a composite matrix increased the thermal stability of HNT-PTh3 compared to pure PTh.

X-ray diffraction

The XRD traces of HNT powder, synthesized PTh and HNT-PTh nanocomposites were determined. As is presented in Fig. 5, pure HNTs, with a crystal size of 58.2 nm and *d*-spacings of 0.445 nm, displayed a characteristic sharp peak at 11.97°2θ, attributed to the tubular morphology of HNTs (Ismail *et al.*, 2008; Rooj *et al.*, 2010). However, the synthesized PTh exhibited a sharp peak at 20°2θ. The XRD traces of the resultant nanocomposites indicated that all typical peaks related to HNTs were present. These findings suggest that the basic crystalline structure of HNTs remained unchanged during ball-milling and polymerization. Furthermore, a distinctive peak of PTh could not be detected in the XRD traces of HNT-PTh, potentially because this peak was covered by the HNT peaks. However, the intensity of the nanocomposite peaks increased with respect to those of pure HNT.

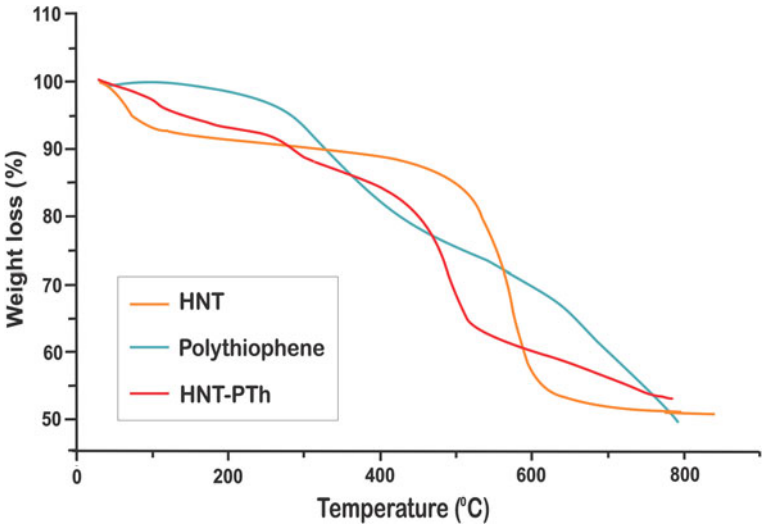

Figure 4. TGA diagrams of HNTs, PTh and HNT-PTh nanocomposites.

https://doi.org/10.1180/clm.2024.2 Published online by Cambridge University Press

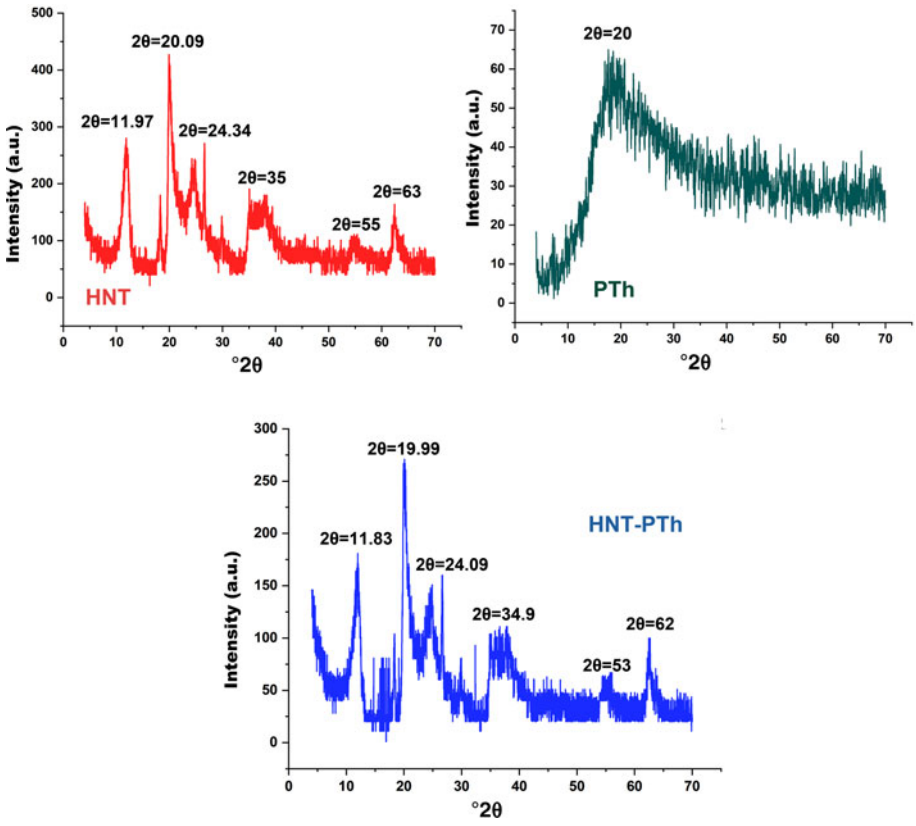

Figure 5. XRD traces of HNTs, PTh and HNT-PTh nanocomposites.

Table 1. Diffraction pattern specifications of HNTs and HNT-PTh nanocomposites.

Characteristic plane Diffraction pattern	001		020		002	
	°2θ	*d* (Å)	°2θ	*d* (Å)	°2θ	*d* (Å)
HNT	11.97	7.430	20.09	4.399	24.34	3.581
HNT-PTh2	11.91	7.456	20.09	4.404	24.33	3.601
HNT-PTh3	11.83	7.471	19.99	4.408	24.09	3.631

The details of the XRD traces and their relative basal spacings are displayed in Table 1. These data indicate that the effective polymerization process and the enhanced polymerization amount resulted in increased peak intensity, as the peaks of HNTs in the nanocomposites were shifted towards lower angles. In addition, the basal spacings of the HNT-PTh nanocomposites increased slightly.

The pH of the point of zero charge

The pHpzc is an important qualitative parameter in the adsorption process, particularly regarding the electrostatic interactions between the adsorbent and adsorbate, demonstrating the surface charge at different pH levels (Fig. 6). In this study, the pHpzc for the HNT-PTh composites was measured to be 7.8. This indicates that the surfaces of the nanocomposites are positively charged below the pHpzc and negatively charged at higher pH values (pH > 7.8).

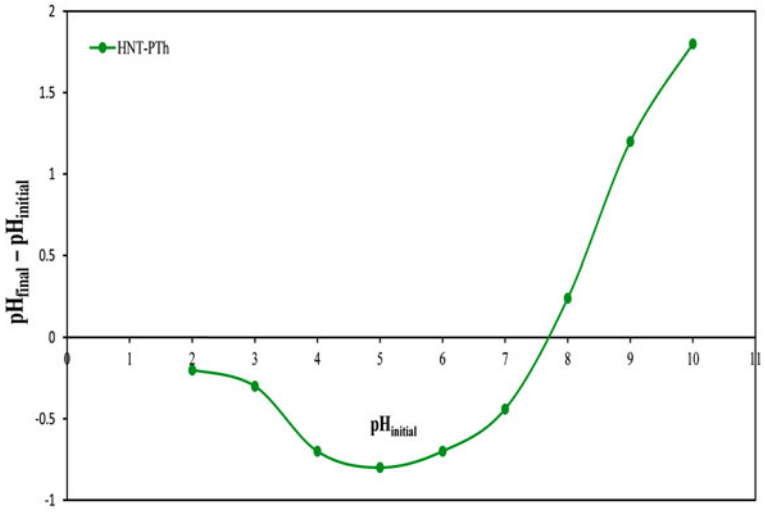

Figure 6. pHpzc graph of HNT-PTh nanocomposites.

https://doi.org/10.1180/clm.2024.2 Published online by Cambridge University Press

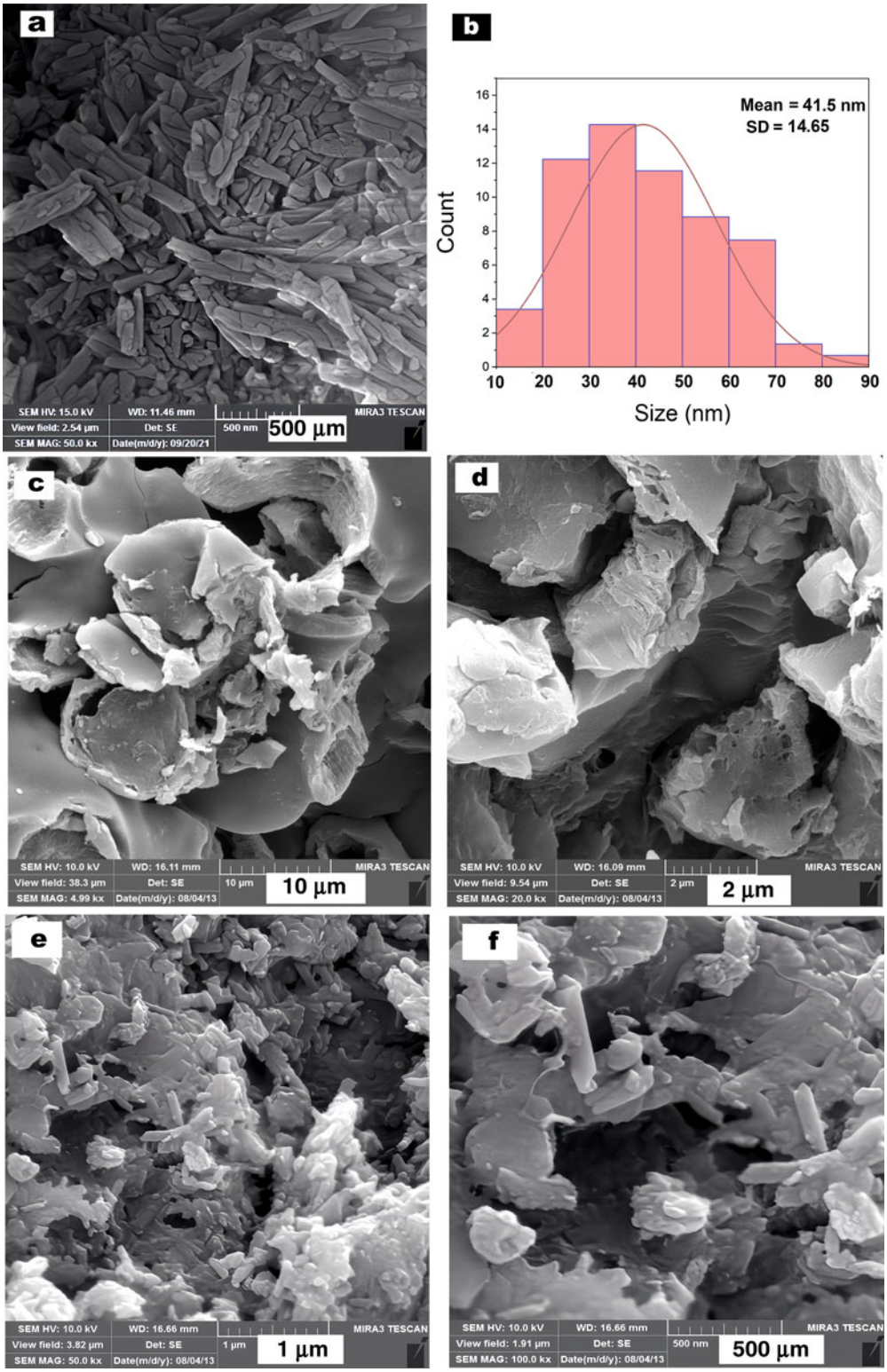

Figure 7. SEM images of ball-milled (a) HNT, (c,d) PTh and (e,f) HNT-PTh nanocomposites. The corresponding diameter distributions of the HNTs are given in (b).

SEM and EDX analyses

The SEM images of ball-milled HNTs, PTh and HNT-PTh are displayed in Fig. 7. The size of HNTs seemed to be reduced whilst preserving their rod and tubular morphology following pre-treatment milling (30 min). The average diameter of ball-milled HNTs was 41.50 ± 14.65 nm (Fig. 5b). The SEM images of prepared PTh exhibited interconnected networks. The HNT-PTh SEM images revealed that there were no drastic

https://doi.org/10.1180/clm.2024.2 Published online by Cambridge University Press

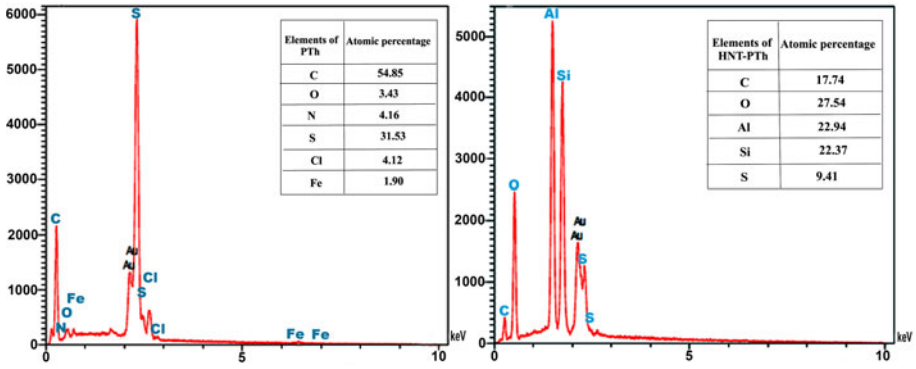

Figure 8. EDX spectra of the PTh (left) and HNT-PTh3 (right) samples.

changes in the morphology of the raw materials of the nanocomposites after polymerization and ball milling compared with HNTs and pure PTh, whereas HNTs maintained their rolled morphology evenly after the polymerization and purification processes.

The presence of HNTs and PTh and their distributions on the surfaces of the composites were determined by evaluating the EDX spectra of the prepared nanocomposites (Fig. 8). As can be seen from the PTh EDX data, the practical percentage ratio of carbon to sulfur in the prepared PTh (C/S = 1.88) is comparable to the theoretical percentage ratio (1.81%). In the EDX spectra of the HNT-PTh nanocomposites, Al (22.94%) and Si (22.37%) originate from the HNTs and S (9.41%) originates from PTh. These results indicate the successful polymerization of thiophene on the surfaces of HNTs in HNT-PTh nanocomposites.

Electrical conductivity

The electrical resistivity of the prepared samples was determined using the standard four-probe method. The highest conductivity was detected for PTh (15×10^{-2} S cm^{-1}). The conductivity of the HNT-PTh nanocomposites was lower (5.2×10^{-3} S cm^{-1}) than that of PTh, which was still higher than that of pure HNT (9×10^{-4} S cm^{-1}). This was due to the presence of insulating HNTs and the high resistance features of mineral clays, which adversely influenced electrical conductivity (Kibria & Hossain, 2017; Zubkiewicz *et al.*, 2020).

Adsorption experiments

After the synthesis and characterization processes, the obtained HNT-PTh nanocomposites were employed for the adsorption of nicotine from an aquatic environment. The removal rate of nicotine was analysed according to variable adsorbent mass, contact time and pH, and the results are reported in Table 2.

Table 2 demonstrates the impacts of pH, contact time and adsorbent dosage on the overall adsorption process and the adsorption capacity. The accessibility of active sites, adsorbent surface charges and ionization of functional groups are strongly impacted by the pH of the uptake process. The pH variation influences the efficiency of adsorption by influencing the repulsion between the functional groups on the adsorbent surface and the pollutant (Khattri & Singh, 2009).

The absorption efficiency of nicotine decreased to 0 at acidic pH (pH 2) for all of the prepared samples. This decline could be related to electrostatic repulsion between the nanocomposite surface and nicotine, as well as the structural decomposition of the alumina layers of halloysite at acidic pH values (Lvov *et al.*, 2016). In addition, an acidic pH resulted in a reduction in the pore volume and size of the HNTs, thereby decreasing adsorption efficacy (Yang *et al.*, 2016). With an increase in pH to 7, the removal rate for fabricated HNT-PTh nanocomposites increased due to the enhanced electrostatic attraction between the negatively charged outer surface of the HNTs and the uncharged (free base) form of nicotine at higher pH values (Zhao & Liu, 2008; Liu *et al.*, 2011; Benowitz, 2022). This electrostatic interaction facilitated the attachment of nicotine onto the nano-halloysite composite. According to the literature, nicotine typically exists in its free, uncharged form at higher pH values (ranging from 7 to 9), and a high percentage of its pyrrolidine nitrogen region demonstrates a positive charge at pH 7 (Bondurant *et al.*, 2001; Benowitz, 2022). Similarly, nicotine adsorption on montmorillonite-based clays was promoted under high-pH conditions (pH ≈ 6–9; Jović-Jovičić *et al.*, 2021).

Table 2. Results of adsorption based on influential variable parameters: pH, contact time and adsorbent dosage.

		Adsorption (%)									
		HNT		PTh		HNT-PTh1		HNT-PTh2		HNT-PTh3	
	Contact time	A	B	A	B	A	B	A	B	A	B
pH 7	5 h	8.86	11.14	0	0	29.31	33.18	36.59	42.27	44.54	47.72
	24 h	15.23	15.23	0	0	35.45	40.68	37.86	41.36	54.40	49.80
pH 9	5 h	0	0	42.00	56.60	35.00	41.50	37.50	44.50	43.70	53.00
	24 h	0	0	45.60	59.00	39.50	42.50	41.50	45.50	48.00	56.50
pH 10	5 h	0	0	10.26	26.84	56.80	60.80	67.10	75.80	70.52	78.15
	24 h	0	0	15.80	37.50	57.63	62.10	68.15	76.30	73.89	78.94
pH 11	5 h	0	0	2.90	8.80	23.53	42.05	29.70	42.05	23.33	42.90
	24 h	0	0	4.11	12.64	29.11	44.41	35.58	42.90	40.00	44.11

A = 50 mg adsorbent; B = 100 mg adsorbent.

https://doi.org/10.1180/clm.2024.2 Published online by Cambridge University Press

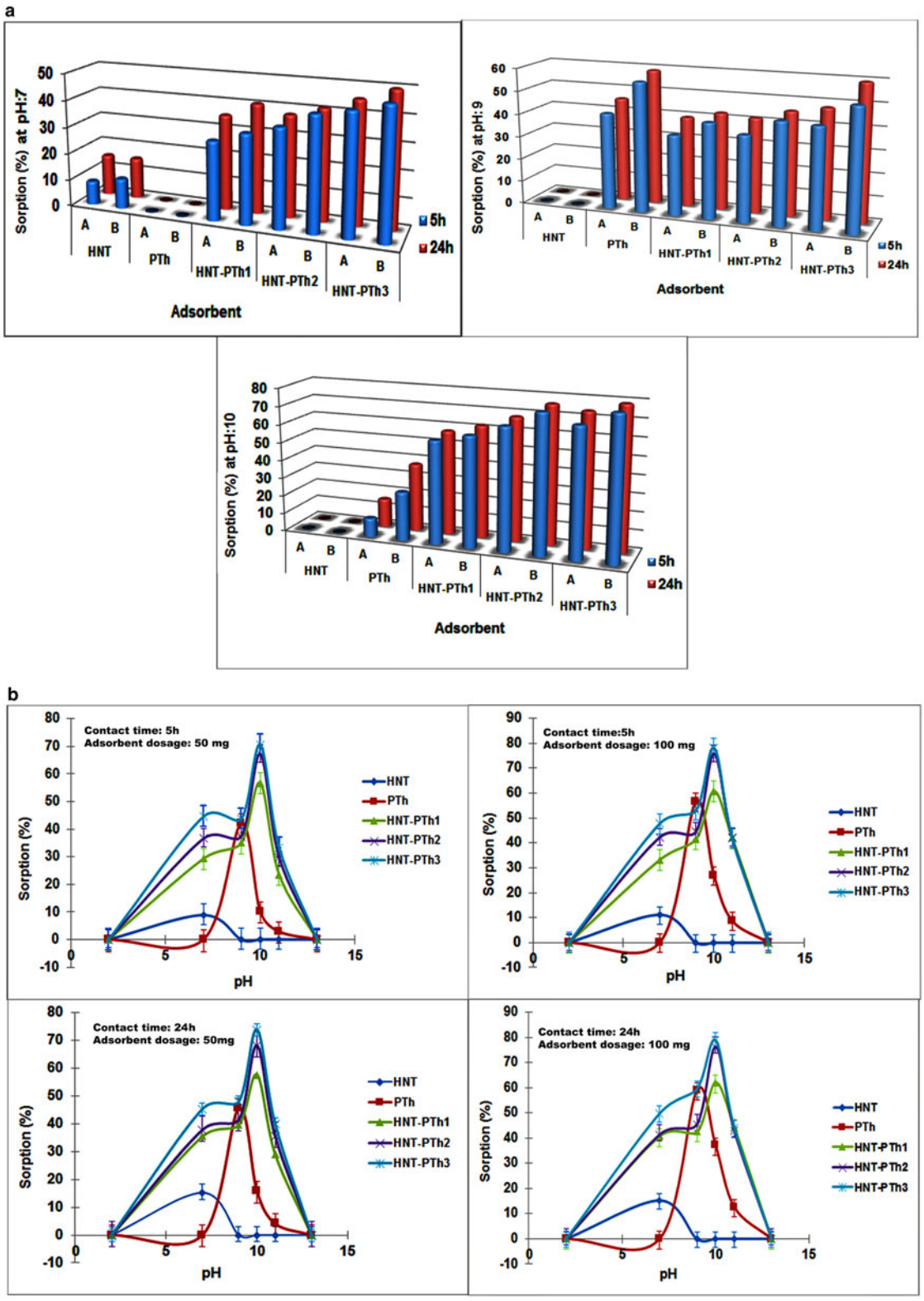

Figure 9. (a) Maximum sorption percentage for the HNTs, PTh and HNT-PTh at pH 7, 9 and 10. (b) Combined influential variable parameters (pH, contact time and adsorbent dosage) on nicotine sorption % (removal percentage), (data are reported as mean ± SD, $n = 3$).

However, as the pH increased up to 13, the adsorption efficiency decreased to 0 for all samples. The decomposition of the octahedral (alumina) and tetrahedral (silica) sheets of HNTs under highly acid or alkaline conditions could be the reason for this reduced adsorption. It was evident that HNTs presented a pH-dependent adsorption profile that was strongly related to the pH-sensitive surface charge (Grim, 1953; White *et al.*, 2012; Same *et al.*, 2022a). The maximum nicotine absorption was

https://doi.org/10.1180/clm.2024.2 Published online by Cambridge University Press

observed for nanocomposites, especially HNT-PTh3 at pH 10. Furthermore, the highest uptake on HNTs was obtained at pH 7, whereas this was obtained at a higher pH (pH 9) for PTh, and both of these uptakes were still lower than the absorption efficacy of the HNT-PTh3 nanocomposites under the same operating parameters. In summary, the use of PTh in composite fabrication, demonstrating higher nicotine uptake at pH 9 and 10 compared to HNTs, improved the removal efficacy. In addition, nicotine removal is notably affected by surface area, and an increased surface area has been previously found to be beneficial for nicotine adsorption in PTh-based composites (Simsek *et al.*, 2021). Thus, the addition of HNTs, known for their high surface area-to-volume ratio, has a positive effect in terms of increasing nicotine adsorption by the nanocomposites.

The interactive effects of adsorbent dosage and contact time on nicotine removal at the aforementioned pH values (7, 9 and 10) are displayed in Fig. 9a. As revealed in Fig. 9a, the use of HNTs during the polymerization process of PTh enhanced the absorption efficiency of the nanocomposites compared to PTh and pure HNT. Moreover, from combined and comparative studies (Fig. 9b & Table 2), it is obvious that the removal efficiency of nicotine (model pollutant) was improved by increasing the contact time and adsorbents mass (up to twofold). This improvement could be related to the easier and greater penetration of nicotine into the adsorbent, which was enhanced by an increase in the number and availability of active sites on the adsorbent surface. Similar trends have been reported in the literature previously (Javanbakht & Ghoreishi, 2017). However, expanding the contact time from 5 to 24 h also resulted in a slight increase in the absorption efficiency, possibly due to the rapid absorption of nicotine by nanocomposites. Reducing the required contact time for rapid absorption is a critical economical parameter for the practical application of adsorbents on an industrial scale (Peighambardoust *et al.*, 2020).

From this combined data, it is obvious that the fabricated HNT-PTh nanocomposites exhibit superior adsorption capacities compared to PTh and pure HNT. Furthermore, the results from the polymerization assays indicate that increasing the polymerization duration on the clay surface and duration of exposure to monomer vapour (up to 2 h) lead to an increase in the adsorption capacity of the HNT-PTh3 nanocomposite compared to the other prepared nanocomposites. It seems that the electrostatic interaction and physical force of attraction are the main mechanisms of nicotine absorption by the nanocomposites. In conclusion, the optimized values for achieving the greatest absorption efficiency (78.94%) were determined to be pH 10, a contact time of 24 h and with 100 mg of adsorbent for HNT-PTh3 nanocomposites (0.268 g after 2 h of polymerization).

Conclusion

In this study, new HNT-PTh nanocomposites were fabricated using vapour-phase polymerization under green and eco-friendly conditions for the removal of nicotine from aqueous solutions. The analysis of the prepared nanocomposites confirmed that HNTs had been successfully integrated into PTh. It was also observed that the presence of HNTs significantly improved the adsorption capacity of the HNT-based nanocomposites. In fact, the resultant nanocomposites exhibited greater adsorption capacities for nicotine compared to PTh alone under all tested conditions. This enhancement can be attributed to the great surface area-to-volume ratio of HNTs and their tubular morphology, which provide a greater number of sites for nicotine adsorption. The effectiveness of this adsorption was influenced by the pH of the solution, the contact time between the nicotine and the adsorbent and the dosage of the nanocomposites. Additionally, it was determined that extending the duration and increasing the amount of vapour-phase polymerization led to greater sorption effectiveness of the nanocomposites at basic pH values. Based on their outstanding ability to adsorb pollutants as well as its easy and scalable preparation process, these eco-friendly HNT-PTh nanocomposites, particularly HNT-PTh3, display significant potential as effective and environmentally safe adsorbents for removing pollutants from contaminated water without releasing further harmful contaminants into the environment. Therefore, it is suggested that the application of green HNT-based polymeric nanocomposites, especially the HNT-PTh3 adsorbent, should be further examined to determine their capacity for adsorbing other toxic chemicals and heavy metals.

Acknowledgements. The authors thank the University of Tabriz for its financial and scientific support.

Conflicts of interest. The authors declare none.

References

Acharya A., Mishra R. & Roy G. (2010) Characterization of CdSe/polythiophene nanocomposite by TGA/DTA, XRD, UV-Vis spectroscopy, SEM-EDXA and FTIR. *Armenian Journal of Physics*, **3**, 195–202.

Anastopoulos I., Pashalidis I., Orfanos A.G., Manariotis I.D., Tatarchuk T., Sellaoui L. *et al.* (2020) Removal of caffeine, nicotine and amoxicillin from (waste) waters by various adsorbents. A review. *Journal of Environmental Management*, **261**, 110236.

Aresta B., Cuocci C., Maggi S., Catellani M., Della C'a N. & Motti E. (2011) *Ab-initio* single crystal structure solution of dihydrodibenzoazepines. Presented at: *XXIV Congresso Nazionale della Società Chimica Italiana, Atti del Congresso*, 11–16 September 2011, Società Chimica Italiana, Università del Salento, Lecce, Italy.

Arsalani N., Zare P. & Namazi H. (2009) Solvent free microwave assisted preparation of new telechelic polymers based on poly(ethylene glycol). *eXPRESS Polymer Letters*, **3**, 429–436.

Benowitz N.L. (2022) The central role of pH in the clinical pharmacology of nicotine: implications for abuse liability, cigarette harm reduction and FDA regulation. *Clinical Pharmacology and Therapeutics*, **111**, 1004.

Bondurant S., Wallace R., Shetty P. & Stratton K. (2001) *Clearing the Smoke: Assessing the Science Base for Tobacco Harm Reduction*. National Academic Press, Washington, DC, USA, 656 pp.

Bordeepong S., Bhongsuwan D., Pungrassami T. & Bhongsuwan T. (2011) Characterization of halloysite from Thung Yai District, Nakhon Si Thammarat Province, in southern Thailand. *Songklanakarin Journal of Science & Technology*, **33**, 599–607.

Capsoni D., Lucini P., Conti D.M., Bianchi M., Maraschi F., De Felice B. *et al.* (2022) Fe_3O_4–halloysite nanotube composites as sustainable adsorbents: efficiency in ofloxacin removal from polluted waters and ecotoxicity. *Nanomaterials*, **12**, 4330.

Cheng H., Frost R.L., Yang J., Liu Q. & He J. (2010) Infrared and infrared emission spectroscopic study of typical Chinese kaolinite and halloysite. *Spectrochimica Acta Part A: Molecular and Biomolecular Spectroscopy*, **77**, 1014–1020.

Cheng C., Song W., Zhao Q. & Zhang H. (2020) Halloysite nanotubes in polymer science: purification, characterization, modification and applications. *Nanotechnology Reviews*, **9**, 323–344.

Dutta K. & Rana D. (2019) Polythiophenes: An emerging class of promising water purifying materials. *European Polymer Journal*, **116**, 370-385.

Enzel P. & Bein T. (1989) Intrazeolite synthesis of polythiophene chains. *Journal of the Chemical Society, Chemical Communications* **18**, 1326–1327.

https://doi.org/10.1180/clm.2024.2 Published online by Cambridge University Press

Ghadiri A.M., Rabiee N., Bagherzadeh M., Kiani M., Fatahi Y., Di Bartolomeo A. *et al.* (2020) Green synthesis of CuO- and Cu_2O-NPs in assistance with high-gravity: the flowering of nanobiotechnology. *Nanotechnology*, **31**, 425101.

Gnanakan S.R.P., Rajasekhar M. & Subramaniaa A. (2009) Synthesis of polythiophene nanoparticles by surfactant-assisted dilute polymerization method for high performance redox supercapacitors. *International Journal of Electrochemical Science*, **4**, 1289–1301.

Grim R.E. (1953) *Clay Mineralogy* (vol. 76). McGraw-Hill, New York, NY, USA, 384 pp.

Haghgir A., Hosseini S.H., Tanzifi M., Yaraki M.T., Bayati B., Saemian T. & Koohi M. (2022) Synthesis of polythiophene/zeolite/iron nanocomposite for adsorptive remediation of azo dye: optimized by Taguchi method. *Chemical Engineering Research and Design*, **183**, 525–537.

Hokmabad V.R., Davaran S., Aghazadeh M., Alizadeh E., Salehi R. & Ramazani A. (2018) A comparison of the effects of silica and hydroxyapatite nanoparticles on poly(ϵ-caprolactone)–poly(ethylene glycol)–poly(ϵ-caprolactone)/chitosan nanofibrous scaffolds for bone tissue engineering. *Tissue Engineering and Regenerative Medicine*, **15**, 735–750.

Holliman P.J., Vaca Velasco B., Butler I., Wijdekop M. & Worsley D.A. (2008) Studies of dye sensitisation kinetics and sorption isotherms of Direct Red 23 on titania. *International Journal of Photoenergy*, **2008**, 827605.

Ismail H., Pasbakhsh P., Fauzi M.A. & Bakar A.A. (2008) Morphological, thermal and tensile properties of halloysite nanotubes filled ethylene propylene diene monomer (EPDM) nanocomposites. *Polymer Testing*, **27**, 841–850.

Javanbakht V. & Ghoreishi S.M. (2017) Application of response surface methodology for optimization of lead removal from an aqueous solution by a novel superparamagnetic nanocomposite. *Adsorption Science & Technology*, **35**, 241–260.

Jin H., Yang D., Wu P. & Zhao M. (2022) Environmental occurrence and ecological risks of psychoactive substances. *Environment International*, **158**, 106970.

Jović-Jovičić N., Mudrinić T., Milutinović Nikolić A., Banković P. & Mojović Z. (2021) The Influence of pH on electrochemical behavior of nicotine–clay based electrodes. *Science of Sintering*, **53**, 535–548.

Khanmohammadi S. & Babazadeh M. (2018) Synthesis of polythiophene/manganese dioxide nanocomposites by *in-situ* core–shell polymerization method and study of their physical properties. *Journal of Nanostructures*, **8**, 366–373.

Khattri S. & Singh M. (2009) Removal of malachite green from dye wastewater using neem sawdust by adsorption. *Journal of Hazardous Materials*, **167**, 1089–1094.

Kibria G. & Hossain S. (2017) Electrical resistivity of compacted clay minerals. *Environmental Geotechnics*, **6**, 18–25.

Koutela N., Fernández E., Saru M.-L. & Psillakis E. (2020) A comprehensive study on the leaching of metals from heated tobacco sticks and cigarettes in water and natural waters. *Science of the Total Environment*, **714**, 136700.

Kumar M., Ambika S., Hassani A. & Nidheesh P. (2023) Waste to catalyst: role of agricultural waste in water and wastewater treatment. *Science of the Total Environment*, **858**, 159762.

Liu R., Zhang B., Mei D., Zhang H. & Liu J. (2011) Adsorption of Methyl Violet from aqueous solution by halloysite nanotubes. *Desalination*, **268**, 111–116.

Lu M.-D. & Yang S.-M. (2005) Syntheses of polythiophene and titania nanotube composites. *Synthetic Metals*, **154**, 73–76.

Luo P., Zhao Y., Zhang B., Liu J., Yang Y. & Liu J. (2010) Study on the adsorption of Neutral Red from aqueous solution onto halloysite nanotubes. *Water Research*, **44**, 1489–1497.

Lvov Y., Wang W., Zhang L. & Fakhrullin R. (2016) Halloysite clay nanotubes for loading and sustained release of functional compounds. *Advanced Materials*, **28**, 1227–1250.

Ma W., Wu H., Higaki Y. & Takahara A. (2018) Halloysite nanotubes: green nanomaterial for functional organic–inorganic nanohybrids. *The Chemical Record*, **18**, 986–999.

Masindi V., Foteinis S., Tekere M. & Ramakokovhu M. (2021) Facile synthesis of halloysite–bentonite clay/magnesite nanocomposite and its application for the removal of chromium ions: adsorption and precipitation process. *Materials Today: Proceedings*, **38**, 1088-1101.

Mohan H., Rajput S.S., Jadhav E.B., Sankhla M.S., Sonone S.S., Jadhav S. & Kumar R. (2021) Ecotoxicity, occurrence, and removal of pharmaceuticals and illicit drugs from aquatic systems. *Biointerface Research in Applied Chemistry*, **11**, 12530.

Nguyen K.D., Trang T.T.C. & Kobayashi T. (2019) Chitin–halloysite nanoclay hydrogel composite adsorbent to aqueous heavy metal ions. *Journal of Applied Polymer Science*, **136**, 47207.

Niu W., Qiu X., Wu P., Guan W., Zhan Y., Jin L. & Zhu N. (2023) Unrolling the tubes of halloysite to form dickite and its application in heavy metal ions removal. *Applied Clay Science*, **231**, 106748.

Nyankson E. & Kumar R. (2019) Removal of water-soluble dyes and pharmaceutical wastes by combining the photocatalytic properties of Ag_3PO_4 with the adsorption properties of halloysite nanotubes. *Materials Today Advances*, **4**, 100025.

Oropesa A.L., Floro A.M. & Palma P. (2017) Toxic potential of the emerging contaminant nicotine to the aquatic ecosystem. *Environmental Science and Pollution Research*, **24**, 16605–16616.

Peighambardoust S.J., Aghamohammadi-Bavil O., Foroutan R. & Arsalani N. (2020) Removal of Malachite Green using carboxymethyl cellulose-g-polyacrylamide/montmorillonite nanocomposite hydrogel. *International Journal of Biological Macromolecules*, **159**, 1122–1131.

Rooj S., Das A., Thakur V., Mahaling R., Bhowmick A.K. & Heinrich G. (2010) Preparation and properties of natural nanocomposites based on natural rubber and naturally occurring halloysite nanotubes. *Materials & Design*, **31**, 2151–2156.

Sahnoune M., Taguet A., Otazaghine B., Kaci M. & Lopez-Cuesta J.-M. (2017) Effects of functionalized halloysite on morphology and properties of polyamide-11/SEBS-g-MA blends. *European Polymer Journal*, **90**, 418–430.

Same S., Nakhjavani S.A., Samee G., Navidi G. & Davaran S. (2022a) Halloysite clay nanotube in regenerative medicine for tissue and wound healing. *Ceramics International*, **48**, 31065–31079.

Same S., Navidi G., Samee G., Abedi F., Aghazadeh M., Milani M. *et al.* (2022b) Gentamycin-loaded halloysite-based hydrogel nanocomposites for bone tissue regeneration: fabrication, evaluation of the antibacterial activity and cell response. *Biomedical Materials*, **17**, 065018.

Simsek E.B., Tuna Ö. & Balta Z. (2021) Exploring nicotine adsorption performance of commercial XAD-4 resin: experimental design, isotherm, kinetic modelling and regeneration. *Journal of Environmental Chemical Engineering*, **9**, 106853.

Sulub S.R., Martinez-Millan W. & Smit M.A. (2009) Study of the catalytic activity for oxygen reduction of polythiophene modified with cobalt or nickel. *International Journal of Electrochemical Science*, **4**, 1015–1027.

Teimuri-Mofrad R., Shahrisa A., Gholamhosseini-Nazari M. & Arsalani N. (2016) Eco-friendly one-pot, three-component synthesis of novel derivatives of kojic acid by the Mannich-type reaction under solvent-free ball-milling conditions. *Research on Chemical Intermediates*, **42**, 3425–3439.

Tierrablanca E., Romero-García J., Roman P. & Cruz-Silva R. (2010) Biomimetic polymerization of aniline using hematin supported on halloysite nanotubes. *Applied Catalysis A: General*, **381**, 267–273.

Verovšek T., Heath D. & Heath E. (2022) Occurrence, fate and determination of tobacco (nicotine) and alcohol (ethanol) residues in waste- and environmental waters. *Trends in Environmental Analytical Chemistry*, **34**, e00164.

White R.D., Bavykin D.V. & Walsh F.C. (2012) The stability of halloysite nanotubes in acidic and alkaline aqueous suspensions. *Nanotechnology*, **23**, 065705.

Yang H., Zhang Y. & Ouyang J. (2016) Physicochemical properties of halloysite. *Developments in Clay Science*, **7**, 67–91.

Yu Y., Ouyang C., Gao Y., Si Z., Chen W., Wang Z. & Xue G. (2005) Synthesis and characterization of carbon nanotube/polypyrrole core–shell nanocomposites *via in situ* inverse microemulsion. *Journal of Polymer Science Part A: Polymer Chemistry*, **43**, 6105–6115.

Zahedi P., Karami Z., Rezaeian I., Jafari S.H., Mahdaviani P., Abdolghaffari A.H. & Abdollahi M. (2012) Preparation and performance evaluation of tetracycline hydrochloride loaded wound dressing mats based on electrospun nanofibrous poly(lactic acid)/poly(ϵ-caprolactone) blends. *Journal of Applied Polymer Science*, **124**, 4174–4183.

Zhao M. & Liu P. (2008) Adsorption behavior of methylene blue on halloysite nanotubes. *Microporous and Mesoporous Materials*, **112**, 419–424.

Zubkiewicz A., Szymczyk A., Franciszczak P., Kochmanska A., Janowska I. & Paszkiewicz S. (2020) Comparing multi-walled carbon nanotubes and halloysite nanotubes as reinforcements in EVA nanocomposites. *Materials*, **13**, 3809.

https://doi.org/10.1180/clm.2024.2 Published online by Cambridge University Press